Lys300 Plays a Major Role in the Catalytic Mechanism of Maize Polyamine Oxidase †

ARTICLE *in* BIOCHEMISTRY · JANUARY 2006

Impact Factor: 3.02 · DOI: 10.1021/bi050983i · Source: PubMed

9 AUTHORS, INCLUDING:

Fabio Polticelli
Università Degli Studi Roma Tre
165 PUBLICATIONS **2,505** CITATIONS
SEE PROFILE

Carmen Faso
University of Zurich
11 PUBLICATIONS **179** CITATIONS
SEE PROFILE

Riccardo Angelini
Università Degli Studi Roma Tre
81 PUBLICATIONS **2,484** CITATIONS
SEE PROFILE

Nigel S Scrutton
The University of Manchester
346 PUBLICATIONS **7,849** CITATIONS
SEE PROFILE

Lys300 Plays a Major Role in the Catalytic Mechanism of Maize Polyamine Oxidase†

Fabio Polticelli,[‡,§] Jaswir Basran,[§,||] Carmen Faso,[‡] Alessandra Cona,[‡] Giovanni Minervini,[‡] Riccardo Angelini,[‡] Rodolfo Federico,[‡] Nigel S. Scrutton,[||,⊥] and Paraskevi Tavladoraki*[,‡]

Department of Biology, University "Roma Tre", Viale G. Marconi 446, 00146 Rome, Italy, and Department of Biochemistry, University of Leicester, Adrian Building, University Road, Leicester LE1 7RH, United Kingdom

Received May 26, 2005; Revised Manuscript Received October 12, 2005

ABSTRACT: Maize polyamine oxidase (MPAO) is a flavin adenine dinucleotide (FAD)-dependent enzyme that catalyses the oxidation of spermine and spermidine at the secondary amino groups. The structure of MPAO indicates a 30-Å long U-shaped tunnel that forms the catalytic site, with residues Glu62 and Glu170 located close to the enzyme-bound FAD and residue Tyr298 in close proximity to Lys300, which in turn is hydrogen-bonded to the flavin N^5 atom via a water molecule (HOH309). To provide insight into the role of these residues in the catalytic mechanism of FAD reduction, we have performed steady-state and stopped-flow studies with wild-type, Glu62Gln, Glu170Gln, Tyr298Phe, and Lys300Met MPAO enzymes. We show that the steady-state enzyme activity is governed by an ionisable group with a macroscopic pK_a of ∼5.8. Kinetic analysis of the Glu62Gln, Glu170Gln, and Tyr298Phe MPAO enzymes have indicated (i) only small perturbations in catalytic activity as a result of mutation and (ii) steady-state pH profiles essentially unaltered when compared to the wild-type enzyme, suggesting that these residues do not play a critical role in the reaction mechanism. These kinetic observations are consistent with computational calculations that suggest that Glu62 and Glu170 are protonated over the pH range accessible to kinetic studies. Substitution of Lys300 with Met in MPAO resulted in a 1400-fold decrease in the rate of flavin reduction and a 160-fold decrease in the equilibrium dissociation constant for the Lys300Met−spermidine complex, consistent with a major role for this residue in the mechanism of substrate oxidation. A sizable solvent isotope effect (SIE = 5) accompanies FAD reduction in the wild-type enzyme and steady-state turnover (SIE = 2.3) of MPAO, consistent with the reductive half-reaction of MPAO making a major contribution to rate limitation in steady-state turnover. Studies using the enzyme-monitored turnover method indicate that oxidized FAD is the prominent form during steady-state turnover, consistent with the reductive half-reaction being rate-limiting. Our studies indicate the importance of Lys300 and probable importance of HOH309 to the mechanism of flavin reduction in MPAO. Possible roles for Lys300 and water in the mechanism of flavin reduction are discussed.

Polyamine oxidase (PAO)[1] is a flavin adenine dinucleotide (FAD)-dependent enzyme involved in the catabolic pathway of polyamines. The enzyme catalyses the oxidation of spermidine (spd), spermine (spm), and/or their acetylated derivatives at the secondary amino groups (*1*, *2*, *3*) (Figure 1). The products of the PAO-catalyzed reaction depend upon the enzyme source and reflects the mode of substrate oxidation. Plant and bacterial PAOs oxidize the carbon on the endo side of the N^5 nitrogens of spd and spm, producing 4-aminobutyraldehyde and 3-(aminopropyl)-4-aminobutyraldehyde, respectively, in addition to 1,3-diaminopropane and H_2O_2 (*1*) (Figure 1). Animal PAOs oxidize the carbon on the exo side of the N^4 nitrogens of N^1-acetyl-spm, N^1-acetyl-spd, and N^1,N^{12}-bis-acetyl-spm to produce spd, put, and N^1-acetyl-spd, respectively, in addition to 3-acetamidopropanal and H_2O_2 (*2*, *4*, *5*). Animal spermine oxidase (SMO) oxidizes the carbon on the exo side of the N^5 nitrogen of spm to produce spd, 3-aminopropanal, and H_2O_2 (*3*, *6*, *7*).

As typically observed in flavin-dependent oxidases, the overall reaction catalyzed by PAO can be divided into a reductive half-reaction, in which the flavin is reduced upon polyamine oxidation, and an oxidative half-reaction, in which the reduced flavin is reoxidized by molecular oxygen with the release of hydrogen peroxide (Figure 1). Polyamine oxidation results in the formation of an imino compound, which is hydrolyzed to produce the final products.

Maize (*Zea mays* L.) PAO (MPAO) is the first PAO for which both the primary (*8*) and tertiary (*9*, *10*) structures

† This work was supported by Consiglio Nazionale delle Ricerche (CNR; Target Project on "BIOTECHNOLOGY" to R.A.), Wellcome Trust (to N.S.S.), the Lister Institute of Preventive Medicine (to N.S.S.), the Biotechnology and Biological Sciences Research Council (to N.S.S.), and a long-term fellowship from the Human Frontier Science Program (to F.P.). Host institution: Department of Biochemistry and Molecular Biophysics, Columbia University, New York.

* To whom correspondence should be addressed: Telephone: +39-0655176352. Fax: +39-0655176321. E-mail: tavlador@uniroma3.it.

‡ University "Roma Tre".

§ These two authors contributed equally to this work.

|| University of Leicester.

⊥ Current address: Faculty of Life Sciences, University of Manchester, P.O. Box 88, Sackville St., Manchester, M60 1QD, U.K.

[1] Abbreviations: FAD, flavin adenine dinucleotide; MAO, monoamine oxidase; MDL72527, *N*,*N*′-bis(2,3-butadienyl)-1,4-butanediamine; MPAO, polyamine oxidase of *Zea mays*; PAO, polyamine oxidase; SMO, spermine oxidase; spd, spermidine; spm, spermine; SIE, solvent isotope effect.

10.1021/bi050983i CCC: $30.25
Published on Web 11/16/2005

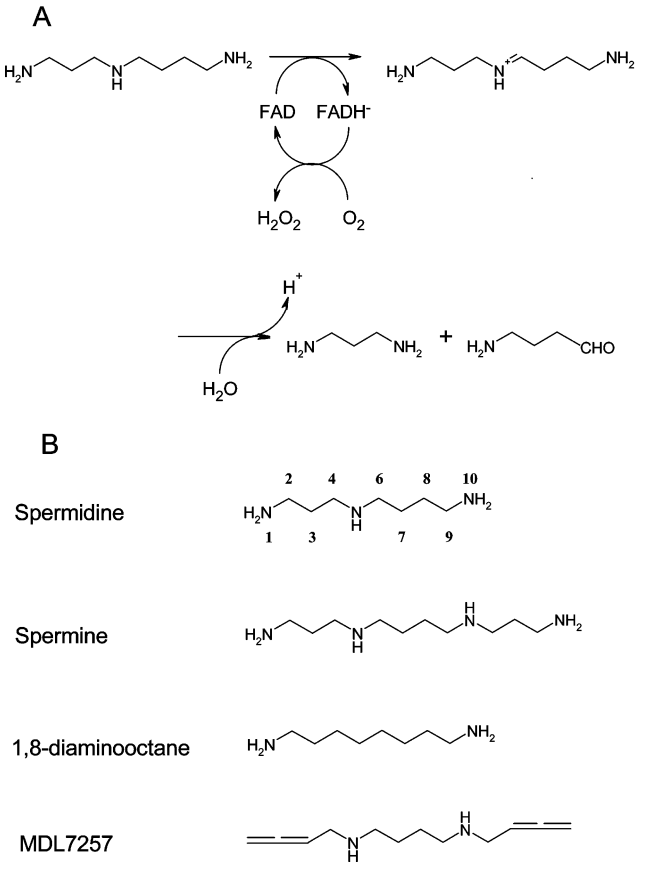

FIGURE 1: MPAO reaction scheme and substrate structure. (A) Reaction scheme for spd oxidation catalyzed by MPAO. (B) Chemical structures of spd, spm, and the MPAO inhibitors 1,8-diaminooctane and MDL72527.

have been determined. MPAO belongs to a new family of FAD-dependent enzymes identified by a 50-residue long signature motif involved in the binding of the ADP-ribityl moiety of FAD (*11*). This family includes oxidoreductases catalyzing a broad spectrum of reactions such as protoporphyrinogen oxidase, phytoene desaturase, and monoamine oxidases (MAO). It is of particular interest that MPAO homology with MAO, an outer membrane mitochondrial enzyme that catalyses the oxidative deamination of monoamine neurotransmitters (*12*) and is involved in depressive disorders and Parkinson's disease (*13*) as well as in apoptosis (*14*), extends beyond the fingerprint motif, raising the possibility of analogies in their catalytic mechanisms (*9*).

The crystal structure of maize PAO has been determined by X-ray diffraction at 1.9 Å resolution in the native oxidized and reduced state as well as in complex with the inhibitors *N*,*N*′-bis(2,3-butadienyl)-1,4-butanediamine (MDL72527), 1,8-diaminooctane (Figure 1), guazatine, and N^1-ethyl-N^{11}-[(cycloheptyl)methyl]-4,8-diazaundacane (*9*, *10*). A prominent feature of the MPAO structure is a 30-Å long U-shaped catalytic tunnel. The innermost part of the tunnel is positioned in front of the flavin isoalloxazine ring and forms the catalytic center. The side chains of Glu62 and Glu170 protrude in front of the flavin, forming the turning point around which the tunnel bends sharply and reverses its direction. Interestingly, these two carboxylate groups are within hydrogen-bonding distance of one another, suggesting that the Glu62−Glu170 pair is protonated (*9*). Moreover, modeling of the MPAO−spm complex (*10*) indicated that Glu62 and Glu170 establish hydrogen bonds with N^5 and N^{14} amino groups of spm, respectively (progressive spm atom numbering starting from the inner side of the MPAO catalytic site). Furthermore, in the crystal structure of the MPAO−MDL72527 complex, the secondary N^{10} amino group of the inhibitor is hydrogen-bonded to the side chain of Tyr298 (*9*). Tyr298 in turn is located in close proximity of Lys300, a residue that is hydrogen-bonded to the N^5 of the FAD via a H_2O molecule (HOH309). HOH309 is the only solvent molecule present inside the catalytic site in the enzyme−substrate or enzyme−inhibitor complexes, while Lys300 is the only active-site residue whose conformation changes upon FAD reduction, possibly allowing a reorientation of HOH309 so that it can now function as a hydrogen-bond acceptor with the protonated N^5 atom of reduced FAD (*10*). Another crucial element of the catalytic tunnel is the presence of residues Phe403 and Tyr439, which are positioned parallel to each other forming an "aromatic sandwich" with the inhibitor. A pair of aromatic residues (Tyr398 and Tyr435) is also present in the catalytic site of the recently solved MAO-B structure (*15*), suggesting that these aromatic rings may be important for flavin-dependent amine oxidation.

The mechanism of flavin-dependent oxidation of amines has been investigated in detail, and several mechanistic proposals have been advanced for substrate dehydrogenation (*16*, *17*). In the hydride transfer mechanism, the direct transfer of a hydride anion from the substrate C−H group to the flavin N^5 position (*18*, *19*) proceeds without the involvement of amino acid functional groups. The aminium cation radical mechanism proposed for MAO by Silverman (*20*) invokes the formation of an aminium cation radical intermediate via an initial single-electron transfer from the amine nitrogen to the oxidized flavin cofactor. In this radical mechanism, several mechanistic possibilities have been considered for the breakdown of the radical intermediate. A mechanism involving hydrogen-atom abstraction from the amine α carbon by an active-site radical species with subsequent electron transfer to the flavin has also been proposed for MAO (*21*, *22*). Alternative mechanisms involve the transient formation of a carbanion through the action of an active-site base, which abstracts the α proton from the substrate. The carbanion intermediate then donates two electrons to the flavin either directly or through a covalent intermediate. Finally, a mechanism involving direct nucleophilic attack by the substrate nitrogen on the flavin C4a atom followed by proton abstraction by an active-site base (*23*) or by flavin N^5 has been suggested for MAO and trimethylamine dehydrogenase (*24*, *25*, *26*). In this mechanism, the substrate nitrogen is deprotonated and a covalent flavin C4a-substrate adduct is formed. Over the years, conflicting views based on a variety of experimental data have been advanced (reviewed in ref *27*). The catalytic mechanism of MPAO has not yet been studied in detail, and the available structural data do not allow us to discriminate between the various proposed mechanisms for flavoenzyme-catalyzed oxidation of amines. However, progress in understanding the catalytic mechanism of MPAO is a promising route for the design of new drugs for cancer therapy.

In this study, we have addressed the functional importance of selected amino acids located in the catalytic tunnel of MPAO (Glu62, Glu170, Tyr298, and Lys300) by site-specific mutagenesis experiments. The mutants have been expressed

in the culture medium of *Pichia pastoris*, and their catalytic parameters have been determined. Our studies indicate that Glu62, Glu170, and Tyr298 residues are not directly involved in the MPAO catalytic mechanism. However, steady-state and stopped-flow kinetic analysis and isotope effect data, together with molecular dynamics simulations and pK_a calculations, for wild-type and the Lys300Met mutant MPAOs, indicate that Lys300 plays a key role in MPAO activity. Possible roles for Lys300 in substrate oxidation are discussed.

EXPERIMENTAL PROCEDURES

Materials. Restriction and DNA-modifying enzymes were purchased from New England Biolabs, Life Technologies, and Promega. All oligonucleotides were synthesized by Life Technologies. DNA sequencing was performed with a Perkin−Elmer ABI Automated DNA Sequencer (model 373A). PCR was carried out in a DNA GeneAmp PCR System2400 (Perkin−Elmer). PCR products were purified following electrophoresis on an agarose gel using the QIAquick gel-extraction kit (Qiagen). Polyamines were purchased from Sigma. All other chemicals were purchased from Bio-Rad, Carlo Erba, and Fluka.

Preparation of the Vector for MPAO Expression in P. pastoris. For MPAO expression in the culture medium of *P. pastoris* (strain X-33), the sequence encoding the MPAO mature protein (*8*) was amplified using pfu Turbo DNA polymerase (Stratagene) and the sequence-specific oligonucleotides MPAO-PIC forward (5′-GGGTATCTCTCGAGAAAAGAGAGGCTGAAGCTGCAACCGTCGGCCCCAGGGTCATCGTCGTCG-3′) and MPAO-PIC reverse (5′-CGGATGCGGATCCTCTAGATCAATGATGATGATGATGATGGTCATACTTTCCCTGACATGGTACTTGC-3′). The amplified fragment was treated for 10 min with Taq polymerase (Polymed) at 72 °C to add 3′ A overhangs and ligated into the pGEM-T Easy vector (Promega) to create the MPAO-pGEMT plasmid. The MPAO cDNA was subcloned into the pPICZαA vector (Invitrogen) between restriction sites *Xho*I and *Xba*I. The MPAO-PIC forward and reverse primers were designed to clone the MPAO cDNA flush with the Kex2 cleavage site in the pPICZαA vector and to insert, at the 3′ terminus of MPAO cDNA, a sequence encoding for a 6-His tag followed by a stop codon. Thus, the MPAO-PIC plasmid was constructed for MPAO ectopic expression in the culture medium of *P. pastoris*.

Site-Directed Mutagenesis. Site-directed mutagenesis was carried out on the plasmid MPAO-pGEMT using the QuikChange Site-Directed Mutagenesis kit (Stratagene) following the protocol of the manufacturers. The mutagenic primers and the corresponding amino acid changes are listed below:

Glu62Gln

(a) 5′-GCCAACTGGGTGCAGGGCGTGAACGGCG-3′

(b) 5′-CGCCGTTCACGCCCTGCACCCAGTTGGC-3′

Glu170Gln

(a) 5′-GGACTACTACAAGTTCGACTACCAGTTCGCGGAGCCGCCG-3′

(b) 5′-CGGCGGCTCCGCGAACTGGTAGTCGAACTTGTAGTAGTCC-3′

Tyr298Phe

(a) 5′-CCAATTCGACATGGCCGTGTTCACCAAGATCTTCCTC-3′

(b) 5′-GAGGAAGATCTTGGTGAACACGGCCATGTCGAATTGG-3′

Lys300Met

(a) 5′-CGACATGGCCGTGTACACCATGATCTTCCTCAAGTTCC-3′

(b) 5′-GGAACTTGAGGAAGATCATGGTGTACACGGCCATGTCG-3′

(a and b indicating the two complementary primers used for each site-directed mutagenesis). Base substitutions are underlined. Mutagenic primers were designed to create a new restriction site, without altering the coding sequence of any other amino acid, for the purpose of screening. The introduction of the mutation was confirmed by sequence analysis. After mutagenesis, the mutated MPAO cDNAs were inserted into the pPICZαA vector following the same experimental procedure as for the wild-type MPAO cDNA.

Expression of Wild-Type and Mutant MPAO Enzymes in P. pastoris. The various MPAO derivatives of the pPICZaA vector were linearized with *Sac*I to target integration at the *AOXI* locus in the *P. pastoris* genome. *P. pastoris* strain X-33 was transformed using the *Pichia* EasyComp kit (Invitrogen). Transformants were plated onto YPDS plates containing 100 μg/mL Zeocin to isolate Zeocin-resistant clones. Several Zeocin-resistant clones were tested for recombinant MPAO expression. Expression in shake flasks was performed following the instructions of the EasySelect *Pichia* Expression kit (Invitrogen). Transformants were initially grown in BMGY medium at 30 °C to an optical density at 600 nm of 2−6. The cells were harvested, and MPAO expression was induced by resuspending them in BMMY medium. Methanol, at a final concentration of 0.5% (v/v), was added to the shake flasks each day. Aliquots of 1 mL were sampled each day to determine the time course and level of expression in the culture medium.

Purification of MPAO. Native MPAO was purified from 8-day-old maize (*Z. mays* L., cultivar Paolo, Monsanto Dekalb) seedlings grown in the dark at 25 °C as described previously (*28*). His-tagged recombinant MPAO was purified from *P. pastoris* culture medium by affinity chromatography using the Ni-NTA resin (QIAGEN). Binding of recombinant MPAO was performed in the presence of 0.5 M NaCl and 100 mM phosphate buffer at pH 6.8 to avoid protein inactivation at higher pH. The column was washed with 50 mM phosphate buffer at pH 6.8, 0.5 M NaCl, and 10 mM imidazole, and the recombinant protein was eluted with 50 mM phosphate buffer at pH 6.0, 0.5 M NaCl, and 0.5 M imidazole and dialyzed against 0.2 M phosphate buffer at pH 6.0 using centrifugal filter devices (Millipore). The enzyme concentration was calculated using a molar extinction coefficient for the oxidized enzyme $\epsilon_{450} = 11\,300\ M^{-1}\ cm^{-1}$.

Determination of MPAO Catalytic Parameters. The catalytic parameters (apparent K_m and k_{cat}) for the oxidation of spd and spm by native, recombinant wild-type and variant MPAO enzymes were determined by following spectropho-

tometrically the formation of a pink adduct ($\epsilon_{515} = 2.6 \times 10^4$ M^{-1} cm^{-1}), as a result of the oxidation of 4-aminoantipyrine and 3,5-dichloro-2-hydroxybenzesulfonic acid catalyzed by horseradish peroxidase in 0.2 M sodium phosphate buffer at pH 6.0 and 25 °C (*29*). One unit of enzyme (U) represents the amount of enzyme catalyzing the oxidation of 1 μmol of substrate/min. k_{cat} values were calculated using saturating concentrations of amine substrates (4 mM) and keeping the O_2 concentration constant at the air-saturated level (apparent k_{cat}). K_m values for recombinant wild-type and variant MPAOs for spd and spm were determined from Michaelis−Menten plots using 4×10^{-3} U of enzyme, a constant O_2 concentration at the air-saturated level, and spd or spm concentrations varying between 1 and 10 μM (apparent K_m). Nonlinear least-squares fitting of data was performed using the Graphpad Prism software.

Studies of the pH dependence of wild-type and variant MPAO activity were conducted in 0.2 M sodium phosphate buffer at 25 °C using the O_2 concentration at the air-saturated level and 4 mM amine substrate. The best fit of the experimental data was carried out by the steepest descent method, using an equation to simulate a two-pK dissociation equilibrium (eq 1)

$$A = A_{max}(-\%pK_1([H^+]/(K_1 + [H^+])) + \%pK_2([H^+]/(K_2 + [H^+]))) \quad (1)$$

where A is the catalytic activity of the enzyme, A_{max} is the maximum catalytic activity, K_1 and K_2 are the equilibrium dissociation constants, $\%pK_1$ and $\%pK_2$ are the relative contributions of each pK to the activity curve, and $\%pK_1 + \%pK_2 = 1$.

Preparation of Anaerobic Samples. Buffers were made anaerobic by bubbling argon gas through solutions for ~2 h. Solutions were then placed in an anaerobic glovebox (Belle Technology Ltd.) overnight to remove any residual traces of oxygen. Samples of purified native MPAO were made anaerobic by passing them through a small gel-filtration (Bio-Rad 10 DG) column housed in the glovebox (Belle Technology Ltd.), which had been pre-equilibrated with anaerobic buffer. Solutions of spd and spm were made by adding the appropriate solid to anaerobic buffer.

Stopped-Flow Kinetic Measurements. Stopped-flow experiments were performed using an Applied Photophysics SX.17 MV or SX.18 MV stopped-flow spectrophotometer. All reactions were performed at 25 °C under anaerobic conditions. For this purpose, the sample-handling unit of the stopped-flow instrument was contained within a Belle Technology glovebox. Multiple-wavelength absorption studies were carried out using a photodiode array detector and X-SCAN software (Applied Photophysics Ltd.) interfaced with the SX.17 MV reaction analyzer. Reactions were carried out in 100 mM potassium phosphate buffer at pH 5.0. Spectral deconvolution was performed by global analysis and numerical integration methods using PROKIN software (Applied Photophysics Ltd.). For single-wavelength studies, data collected at 450 nm were analyzed using nonlinear least-squares regression analysis on an Archimedes 410-1 microcomputer with Spectrakinetics software (Applied Photophysics Ltd.). Experiments were performed by mixing purified native or mutant MPAO (5 μM) contained in 100 mM phosphate buffer of the desired pH with an equal volume of substrate at the desired concentration in the same buffer. The concentration of the substrate was always at least 10-fold greater than that of MPAO, thereby ensuring pseudo-first-order conditions.

In single-wavelength experiments, the transients collected at A_{450} were biphasic and were fitted using the standard double-exponential expression (eq 2)

$$A_{450} = C_1 e^{-k_{obs1}t} + C_2 e^{-k_{obs2}t} + b \quad (2)$$

where k_{obs1} and k_{obs2} are the observed rate constants for the fast and slow phases, respectively, C_1 and C_2 are the relative amplitude values for the two phases, and b is an offset value to account for a nonzero baseline. Rate constants for the fast phase were dependent upon the substrate concentration, and the reaction sequence was modeled according to the following scheme:

$$A + B \underset{k_2}{\overset{k_1}{\rightleftarrows}} C \xrightarrow{k_3} D$$

where A is oxidized MPAO, B is the substrate (spd or spm), C is the Michaelis complex, and D is a two-electron-reduced form of MPAO. Data were fitted to eq 3

$$k_{obs} = \frac{k_3[S]}{K_d + [S]} \quad (3)$$

All curve fitting was performed using the Grafit version 3 software package (*30*).

Enzyme-Monitored Turnover Experiments. Steady-state measurements were performed using the enzyme-monitored turnover method as described by Gibson et al. for reactions catalyzed by glucose oxidase (*31*). Reactions were performed aerobically in an Applied Photophysics SX.18 MV reaction analyzer. Experiments were carried out in 100 mM potassium phosphate buffer at pH (D) 4.0. Data analysis was essentially as described elsewhere (*31*).

Solvent Isotope Effect (SIE) Experiments. For experiments conducted in ^2H_2O, all buffer components and substrates were dissolved in ^2H_2O and the pD of the solution was calculated by the addition of 0.4 to the pH-meter reading to correct for the isotope effect on the electrode. Stock solutions of MPAO were exhaustively dialyzed against 50 mM NaH_2PO_4 buffer at pD 5.5 containing 300 mM NaCl. The preparation of anaerobic samples was the same as for the H_2O experiments.

Modeling of Wild-Type and Mutant MPAO−Substrate Complexes. The structures of the MPAO−spm and MPAO−spd complexes were modeled using the structure of the MPAO−MDL72527 complex [PDB code 1B5Q (*9*)] and that of the MPAO−1,8-diaminooctane complex [PDB code 1H83 (*10*)], respectively. In detail, the structures of MDL72527 and 1,8-diaminooctane bound in the MPAO active site were modified into that of spm and spd, respectively, using the biopolymer module of InsightII (Molecular Simulations Inc.), to obtain the wild-type MPAO−spm and MPAO−spd complexes. The wild-type MPAO−substrate complexes were then used to model Lys300Met MPAO−substrate complexes by simple substitution of Lys300 with Met using InsightII

Table 1: Kinetic Constants of spd and spm Oxidation by Wild-Type and Mutant Forms of MPAO Expressed in *P. pastoris*

MPAO	k_{cat}[a] (spd) (s^{-1})	k_{cat}[a] (spm) (s^{-1})	k_{cat} (spd)/ k_{cat} (spm)[a]	K_m[a] (spd) (μM)	K_m[a] (spm) (μM)	k_{cat}/K_m (spd) (s^{-1} μM^{-1})
wild-type	50.2 ± 6.3 (100)[b]	32.9 ± 1.1	1.5 ± 0.1	2.1 ± 0.3	1.6 ± 0.4	23.9
Glu62Gln	8.3 ± 0.8 (16.5)	2.8 ± 0.4	2.8 ± 0.4	24.6 ± 2.0	14.7 ± 2.5	0.3
Glu170Gln	17.3 ± 2.1 (34.5)	4.6 ± 0.8	3.5 ± 0.3	16.7 ± 1.6	12.5 ± 1.8	1.0
Tyr298Phe	16.5 ± 0.6 (32.9)	7.7 ± 0.6	2.0 ± 0.1	0.7 ± 0.2	1.2 ± 0.2	23.6
Lys300Met	$(4.4 \pm 0.4) \times 10^{-3}$	$(5.3 \pm 0.4) \times 10^{-3}$	0.9 ± 0.2	ND[c]	ND	ND
native	55.1 ± 1.2 (109.8)	39.3 ± 2.6	1.4 ± 0.4	1.7 ± 0.4	1.4 ± 0.1	32.4

[a] Enzymatic activity of native and recombinant MPAO has been determined in 0.2 M sodium phosphate buffer at pH 6.0, using a constant O_2 concentration at the air-saturated level and an amine substrate concentration either saturating (for apparent k_{cat} determination) or varying between 1 and 10 μM (for apparent K_m determination). Data are mean ± SEM of at least three independent experiments. [b] Percentage of wild-type values is shown in parentheses. [c] ND = not determined.

and choosing the appropriate Met rotamer to avoid bumps with neighboring residues.

Molecular Dynamics Simulations. The wild-type and mutant MPAO−substrate complexes were equilibrated in water by molecular dynamics simulations in explicit solvent using the CHARMM macromolecular mechanics package (*32*) and the CHARMM22 parameters and force field (*33*). The three-site TIP3p model (*34*) was used for water molecules. In detail, hydrogen atoms were added to the modeled complexes using the routine HBUILD of the CHARMM package. The minimized complexes were placed in a truncated octahedron, constructed from a cubic volume of water molecules of dimension 77.758 × 77.758 × 77.758 Å, and water molecules overlapping with protein−substrate atoms (cutoff = 2.8 Å) were removed. Solvated structures, containing approximately 5100 solvent molecules, were energy-minimized by applying a harmonic force of 10 kcal/mol to non-hydrogen atoms of the complexes to allow reorganization of the solvent. Minimized solvated structures were then subjected to a molecular dynamics simulation at 298 K in the microcanonical ensemble, after a heating run of 10 ps, during which the temperature was gradually increased from 0 to 298 K. The simulation time step was set to 0.002 ps. Equilibrium, as judged by convergence of the root-mean-square deviation (rmsd) of the position of non-hydrogen atoms from the initial structures (Δrmsd < 0.05 Å), was reached in all of the complexes after approximately 60 ps.

Calculation of pK_a Values. pK_a values of the ionisable residues of wild-type and mutant MPAOs in the free state and in complex with the substrates have been calculated using MCCE (Multiconformation continuum electrostatics), which combines continuum electrostatics and molecular mechanics force fields in Monte Carlo sampling to simultaneously calculate side-chain ionization and conformation (*35*−*37*). A test of this method carried out calculating the pK_a of 166 residues in 12 proteins showed that the root-mean-square error between calculated and experimental pK_a values was only 0.83 pH units, with more than 90% of the calculated values displaying errors lower than 1 pH unit (*37*).

RESULTS

Characterization of Site-Directed MPAO Mutants. Analysis of the active-site structure of free and inhibitor-bound MPAO (*9*, *10*) led to the hypothesis that residues Glu62, Glu170, Tyr298, and Lys300 might be involved in the catalytic mechanism of this enzyme, either by providing hydrogen bonds to the substrate and/or acting as bases during catalysis. To elucidate the role of these amino acids in the catalytic mechanism of MPAO, we obtained the following site-directed mutants of MPAO: Glu62Gln, Glu170Gln, Tyr298Phe, and Lys300Met.

To enable a biochemical characterization of the MPAO mutants, we examined the possibility of obtaining high expression levels of recombinant MPAO in the culture medium of *P. pastoris* using the pPICZaA vector. To facilitate protein purification, a 6-His tag has been added to the C terminus of the recombinant protein, which, from the crystal structure of the enzyme, is predicted to be well-exposed to solvent (*9*). High expression levels of recombinant MPAO in the *P. pastoris* culture medium were observed. The highest expression levels were approximately 4 mg of enzyme/L of culture 5 days after induction. Biochemical characterization of wild-type enzyme expressed in *P. pastoris* indicated that apparent k_{cat} and K_m values were similar to those measured for the native enzyme (Table 1). These data suggest, therefore, that (i) the presence of the 6-His tag on the C terminus of the enzyme and (ii) the possibility of different glycosylation patterns in the yeast-expressed recombinant protein do not interfere appreciably with the catalytic activity.

Analysis of the steady-state catalytic parameters for the MPAO variants demonstrated that substitution of Glu62 or Glu170 with Gln results in only a moderate change of the enzyme activity and apparent Michaelis constants (Table 1). These data indicate that the side chains of Glu62 and Glu170 do not play a major role in the catalytic mechanism of the enzyme. Moreover, the moderate affect on measured kinetic parameters following mutation suggests that the two Glu residues are protonated at physiological pH. Substitution of Tyr298 with Phe likewise did not substantially alter either the specific activity or the apparent Michaelis constant (Table 1), consistent with the hydroxyl group of the Tyr298 side chain not playing a major role in the catalytic mechanism of MPAO. Analysis of the reaction products of the three MPAO mutants indicated that the products of the reaction were identical to those formed with the wild-type enzyme (data not shown), consistent with the retention of the same catalytic mechanism in the mutant MPAO enzymes.

The pH dependence of the catalytic activity of the recombinant MPAO variants was determined using spd (Figure 2 and Table 2) and spm as a substrate (data not shown). The results obtained show that for both substrates the catalytic activity of wild-type recombinant MPAOs changes with pH as for the native enzyme purified from

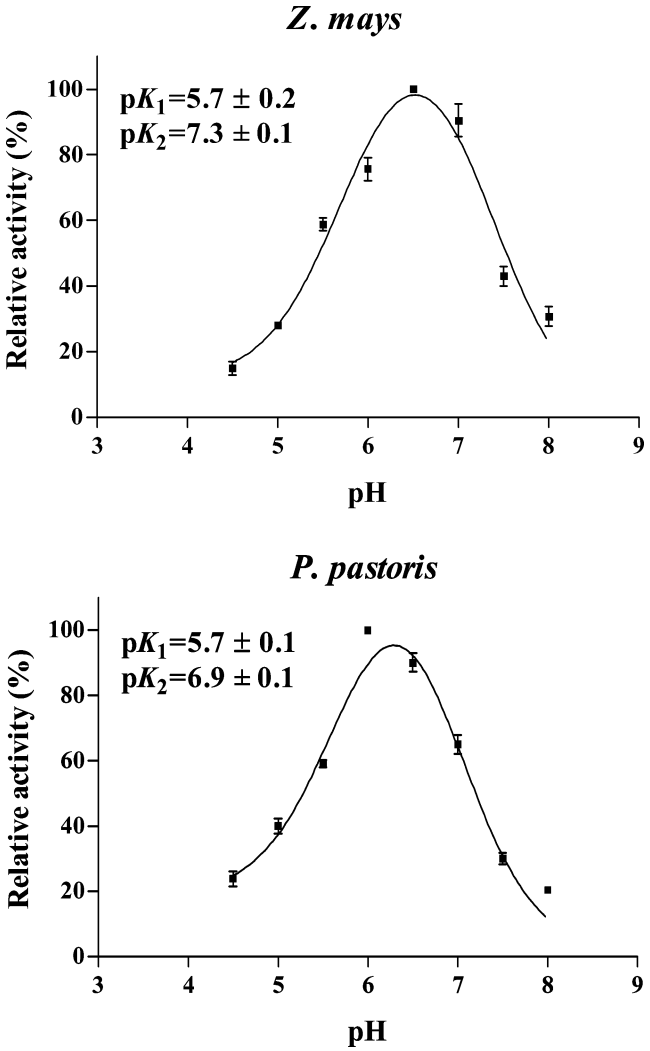

FIGURE 2: Relative catalytic activity of wild-type MPAO expressed in plants of *Z. mays* and in the culture medium of *P. pastoris* as a function of pH. Apparent k_{cat} values of wild-type MPAO purified from plants of *Z. mays* and the culture medium of *P. pastoris* toward spd were calculated at various pH values using saturating concentrations of amine substrate and O_2. Data are expressed as a percent of the maximum activity. Continuous lines represent the best fit of the experimental data. Each point represents the mean value from at least three independent experiments, and the bars indicate the standard error.

Table 2: pH Dependence of the Catalytic Activity of MPAO Variants Expressed in *P. pastoris*[a]

MPAO	pH max[b]	pK_1	pK_2
wild-type	6.0	5.7 ± 0.1	6.9 ± 0.2
Glu62Gln	6.0	5.2 ± 0.1	6.5 ± 0.1
Glu170Gln	6.5	6.1 ± 0.2	6.9 ± 0.2
Tyr298Phe	5.5	5.1 ± 0.3	6.5 ± 0.1

[a] Activity toward spd was determined in 0.2 M sodium phosphate buffer at various pH values. p*K* values are mean ± SEM of three independent experiments. [b] pH of maximum enzyme activity.

maize. In particular, the catalytic activity increases with pH, reaching a maximum at around pH 6.5 (Figure 2). At higher pH values, the catalytic activity of the wild-type enzymes diminishes substantially (Figure 2). Despite a slight difference in the activity pH optimum and assuming no change in the rate-limiting step as a function of pH, the pH dependence of the catalytic activity for both the native and recombinant wild-type enzymes can be described in terms of deprotonation of an ionisable group with a pK_a value of 5.7−5.8, responsible for the acidic side of the bell-shaped dependence (pK_1; Figure 2), and an ionisable group with a pK_a value of 6.9, responsible for the alkaline side (pK_2; Figure 2). A similar bell-shaped dependence of catalytic activity on pH was also observed for the Glu62Gln, Glu170Gln, and Tyr298Phe MPAO enzymes. As shown in Table 2, the substitution of Glu62 and Glu170 residues with a Gln residue and of Tyr298 with a Phe residue did not significantly influence the p*K* values. The side chains of the two active-site glutamates and the phenolic hydroxyl group of Tyr298 are therefore not attributable to the ionisable group responsible for the observed pH dependence of MPAO activity.

Stopped-Flow Studies of Flavin Reduction by spd and spm. We have performed stopped-flow kinetic studies of FAD reduction by spd and spm to provide insight into the mechanism of the reductive half-reaction of MPAO. The reductive half-reaction of native MPAO purified from maize plants using spd as the substrate was initially studied at 25 °C under pseudo-first-order conditions using photodiode array detection (Figure 3). Reactions were performed under strictly anaerobic conditions. The time-dependent spectra (collected over 500 ms) were fitted globally by numerical integration methods using Prokin software (Applied Photophysics). Data were best fitted to a two-step model (A → B → C). Species A has absorption characteristics of oxidized flavin and clearly represents the oxidized enzyme (probably as the substrate Michaelis complex). In the conversion of species A to species B, the flavin redox center is reduced and the spectrum is typical of the dihydroflavin form. A small spectral change occurs in the conversion of species B to species C, the origin of which is uncertain. However, the flavin clearly remains reduced, and formation of species C is not catalytically important in steady-state reactions (see below). Results obtained from our multiple wavelength absorption experiments are in agreement with recent reductive half-reaction studies carried out with mouse PAO (*38*). In the mouse enzyme flavin reduction using the slow substrate, N^1,N^{12}-bisethylspermine proceeded in a single step with the formation of the reduced enzyme occurring without the formation of any detectable intermediates. Photoreduction of the MPAO-bound FAD was also monitored using the photodiode array detector of the stopped-flow apparatus. These experiments indicated that photobleaching of the enzyme-bound flavin did occur, albeit slowly, and that complete reduction was obtained only after prolonged exposure to light (>500 s). The longer time scale for photoreduction of the enzyme does not complicate analysis of flavin reduction by the substrate over relatively shorter time scales using diode array stopped-flow spectroscopy. Qualitatively similar spectral changes were observed in the pH range of 4.0−5.5 (not shown); studies at pH values >5.5 were not possible, because flavin reduction rates were too fast to be monitored by the stopped-flow method.

Single-wavelength stopped-flow studies were performed at 450 nm to investigate the dependence of the rate constants for individual phases seen in the diode array experiments on the substrate concentration. Reactions were performed initially in 100 mM potassium phosphate buffer at pH 6.5 (the optimum pH for enzyme activity determined from steady-state kinetic experiments) and 25 °C, but rates of

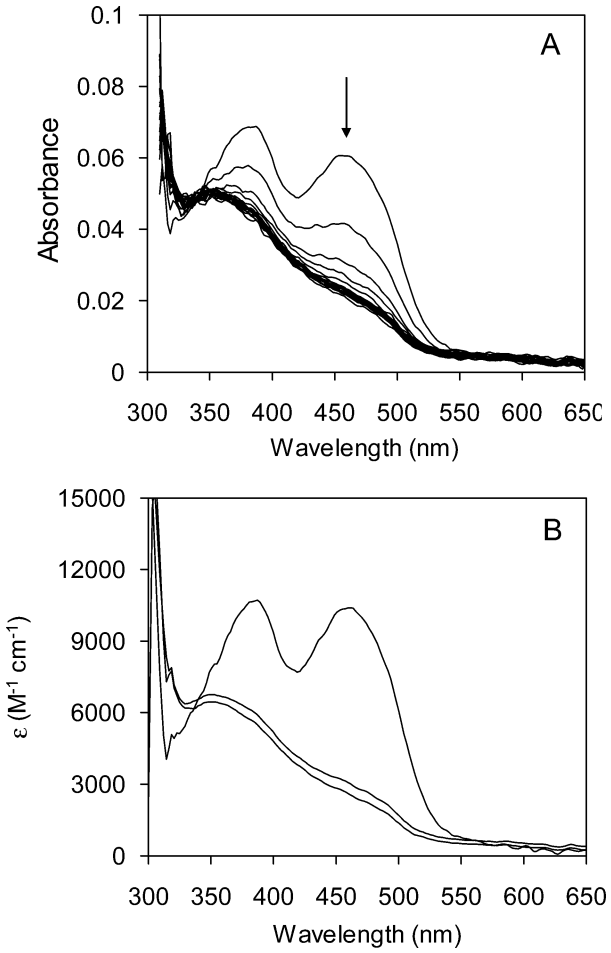

FIGURE 3: Reduction of MPAO monitored by photodiode array detection. Conditions: 8 μM enzyme concentration, 1 mM spd concentration, and 100 mM potassium phosphate buffer at pH 5.0 and 25 °C. (A) Time-dependent spectral changes on mixing purified native MPAO with spd. For clarity, not all spectra are shown. (B) Deconvoluted spectra obtained by fitting the data in A to a two-step model A → B → C. The rate constants (s^{-1}; obtained from global fitting) are A → B, 146 ± 1.4; B → C, 1.7 ± 0.3. Upper spectrum, species A; intermediate spectrum, species B; lower spectrum, species C.

flavin reduction were found to be too fast (>650 s^{-1}) for accurate analysis by the stopped-flow method. Single-wavelength stopped-flow studies were therefore performed at pH 4.0, where accurate analysis of flavin reduction by the substrate was possible. Consistent with photodiode array data, absorption changes monitored at 450 nm were biphasic with spd (Figure 4A) and with spm (data not shown), and the absorption change associated with each kinetic phase was as observed in diode array studies (Figure 3). The fast phase reporting on flavin reduction (conversion of species A → B) was found to be dependent upon the substrate concentration with spd and spm. The limiting rate of flavin reduction, k_{lim}, and the equilibrium dissociation constant for the enzyme−substrate complex (K_d) was calculated using eq 3 (parts B and C of Figure 4). The limiting rate for flavin reduction in the enzyme−substrate complex was calculated to be 57.4 ± 1.4 s^{-1} for spd and 96.5 ± 4.4 s^{-1} for spm. The K_d for the enzyme−substrate complex was 2.9 ± 0.22 and 1.1 ± 0.15 mM for the MPAO−spd and MPAO−spm complexes, respectively. The observed rate constants for the slow phases (~3−8 s^{-1} for both spm and spd, i.e., conversion of species B → species C) were found to be independent of the substrate concentration.

Steady-State Reactions of MPAO. Enzyme-monitored turnover experiments (*31*) at pH 4.0 were performed to derive additional information on the reduction state of the enzyme during steady-state turnover and to enable a comparison with stopped-flow data. Kinetic traces for the steady-state turnover of MPAO in the presence of different concentrations of spd are shown in parts a and b of Figure 5. In each experiment at 450 nm, there is a rapid and partial decrease in the absorption followed by the steady-state phase. The steady-state phase is followed by a final decrease in absorption as the fully reduced (dihydroflavin) enzyme is formed, owing to depletion of molecular oxygen. The spectral forms of MPAO at different points in the multiple turnover analysis are shown in the inset of Figure 5a. Initially, the enzyme is in the oxidized form (point A on the trace). After rapid reduction by the substrate and establishment of the steady-state phase (point B on the trace), the enzyme remains predominately in the oxidized form. After depletion of molecular oxygen (point C on the trace), the enzyme-bound flavin is converted to the dihydroflavin. Kinetic traces obtained at different concentrations of reducing substrate are shown in Figure 5b. The analysis of these traces was performed as described by Gibson and co-workers (*31*). The traces represent a record of the rate of catalysis as a continuous function of the oxygen concentration. Figure 5c indicates that a series of parallel lines are obtained on plotting the reciprocal of the turnover number versus the reciprocal of the oxygen concentration. A secondary plot of the ordinate intercept versus the spd concentration is shown in Figure 5d. The reciprocal of the ordinate intercept of this secondary plot (31.0 ± 1.9 s^{-1}) is the true turnover number, k_{cat}, for the steady-state reaction. The true K_m for spd (2.12 ± 0.20 mM) is derived from this plot by dividing the value of the gradient by the ordinate intercept. The true K_m for molecular oxygen (0.083 ± 0.007 mM) was obtained by taking the slope of any line in Figure 5c (in this case, the 1 mM spd line) divided by the intercept of the line in Figure 5c.

The K_m for spd at pH 4.0 (2.1 mM) is comparable to the K_d value (2.9 mM) for this substrate calculated from single-turnover experiments at the same pH. The turnover number determined from the steady-state experiments is however slightly lower than the limiting rate of flavin reduction (31 cf. 57 s^{-1}) under the same conditions (pH 4.0), suggesting that reduction of the flavin is probably the main contributing factor to rate limitation in the steady-state. This was confirmed by monitoring the spectral changes that occur during the steady-state reaction (Figure 5a). These experiments clearly demonstrate that it is the oxidized form of the enzyme that accumulates during steady-state turnover (spectrum B; inset of Figure 5a), consistent with flavin reduction being the main contributor to rate limitation in the overall catalysis. Species C, observed at the end of the enzyme-monitored turnover experiments has a characteristic dihydroflavin spectrum. The spectral form of this enzyme species is similar to that observed at the end of the anaerobic single-turnover experiments (Figure 3B).

SIE. A water molecule (HOH309) is hydrogen-bonded to Lys300 in the structure of MPAO, and this is the only water molecule present in the active site in structures of enzyme−substrate and enzyme−inhibitor complexes. To investigate

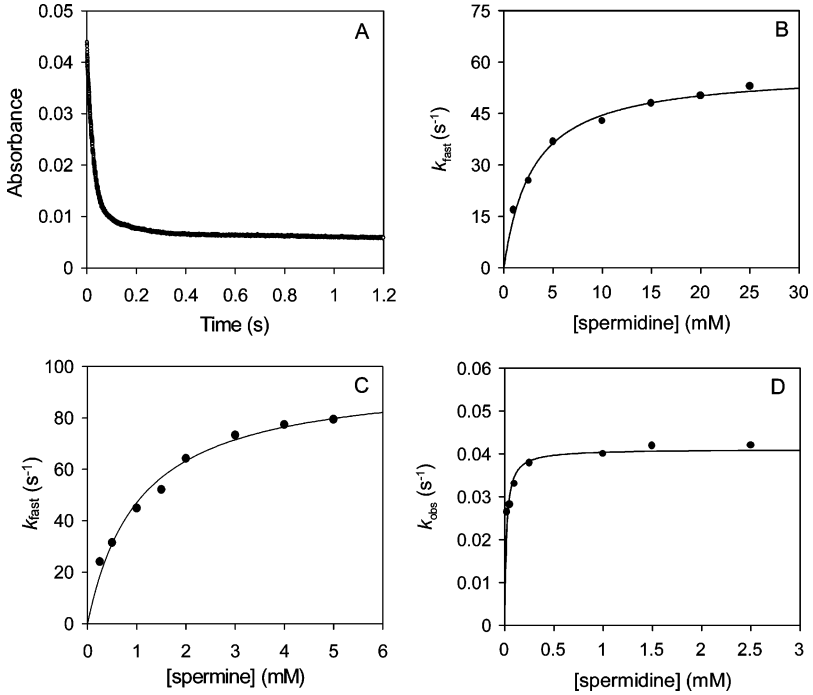

FIGURE 4: Stopped-flow data for enzyme reduction by the substrate. (A) Transient obtained at 450 nm for wild-type MPAO. Conditions: 5 μM enzyme concentration and 20 mM spd concentration at pH 4.0 and 25 °C. Fitting to a biphasic expression yielded rate constants of 50.6 ± 0.2 and 4.5 ± 0.1 s^{-1}. (B) Plot of observed fast rate constant obtained from stopped-flow transients collected at 450 nm against the spd concentration for wild-type MPAO. Data shown are those collected at pH 4.0 and 25 °C. (C) Plot of observed fast rate constant obtained from stopped-flow transients collected at 450 nm against the spm concentration for wild-type MPAO. Data shown are those collected at pH 4.0 and 25 °C. (D) Plot of observed rate constant obtained from stopped-flow transients collected at 450 nm against the spd concentration for Lys300Met MPAO (reaction conditions: same as for wild-type MPAO).

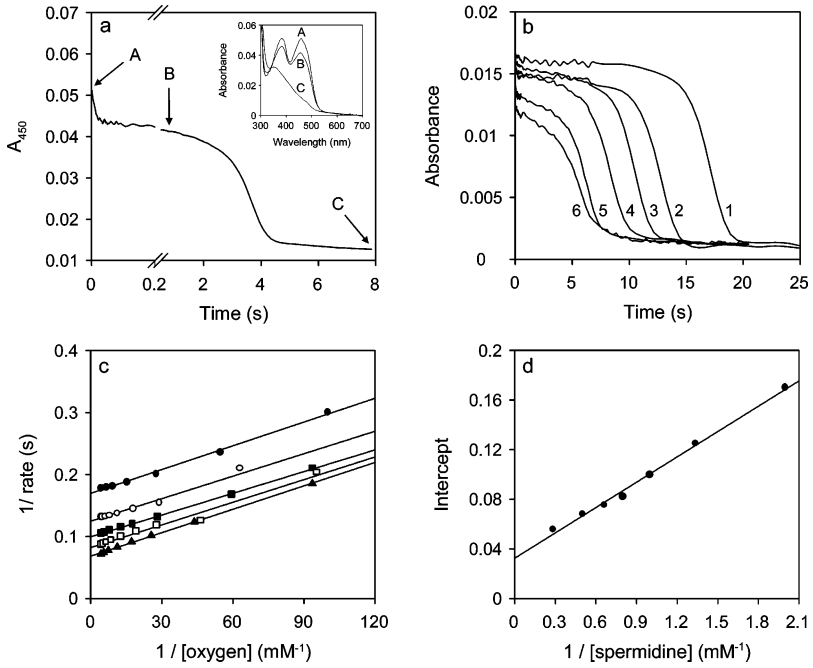

FIGURE 5: Enzyme-monitored steady-state turnover of MPAO. (a) Enzyme (5 μM of native enzyme) reacted with 10 mM spd in 100 mM phosphate buffer at pH 4.0 and 25 °C. The course of reaction was monitored at 450 nm versus time. The arrow A shows the initial absorption, which is initially rapidly bleached as a result of flavin reduction, prior to establishing steady-state conditions. (Inset) Spectrum of the enzyme recorded with a photodiode array detector at the indicated selected points in the time course of the main panel; the oxygen concentration was 0.258 mM. (b) Progress curves obtained at various spd concentrations. Curves 1−6 are for spd concentrations of 0.5, 0.75, 1, 1.5, 3.5, and 5 mM, respectively. Only selected progress curves are shown. (c) Plot of 1/rate versus 1/oxygen concentration. (●) 1 mM, (○) 2 mM, (■) 5 mM, (□) 20 mM, (▲) 30 mM spd. (d) Plot of the intercept of the plot shown in c versus 1/spd concentration.

the potential role of this water molecule in catalysis, we performed stopped-flow studies of flavin reduction by spd in ^2H_2O at pD 4.0. As in H_2O, the transients collected at 450 nm in ^2H_2O were biphasic in nature. The rate of flavin reduction (fast phase) was dependent upon the substrate concentration, and the rate of the slow phase was independent

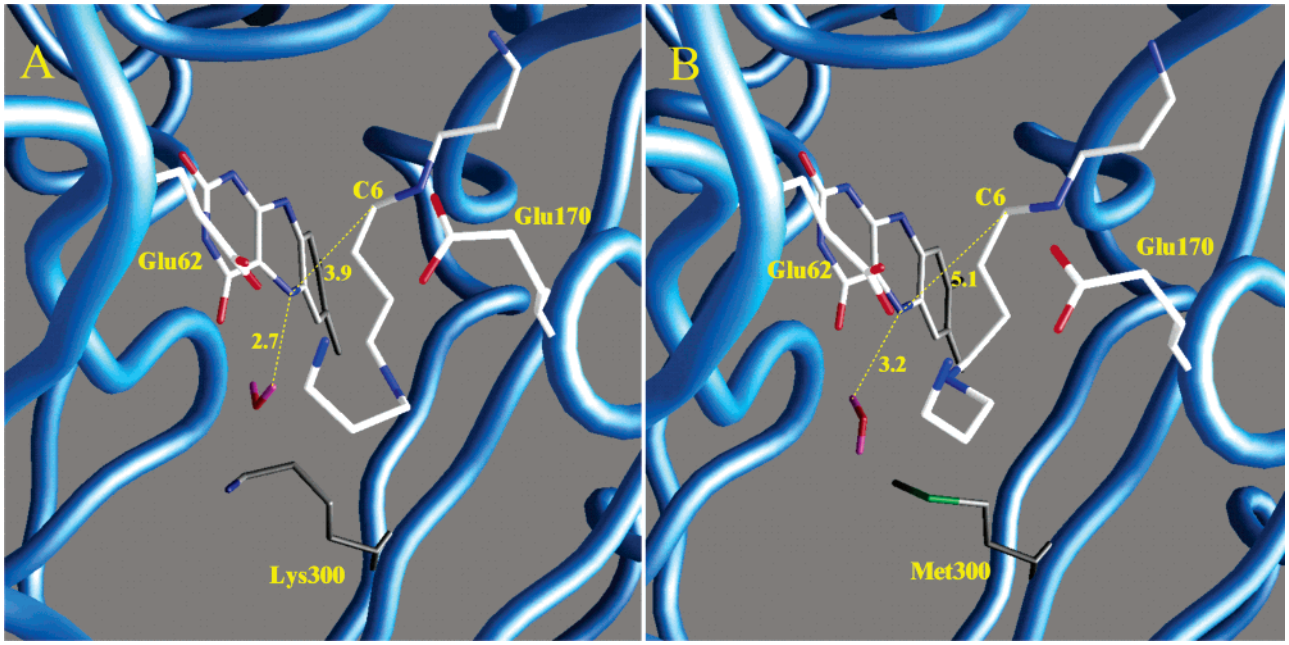

FIGURE 6: Schematic representation of the active site of wild-type and Lys300Met MPAO in complex with spm. (A) Wild-type MPAO−spm complex. (B) Lys300Met MPAO−spm complex. For clarity, only the isoalloxazine ring of FAD is shown. Distances between the C^6 atom of spm and the N^5 atom of FAD and between HOH309 and the N^5 atom of FAD are indicated by dashed lines. For details see the text. The figure was drawn with Grasp (*49*).

of the substrate concentration. The rate of flavin reduction in MPAO is slower in ^2H_2O ($k_{lim} = 11.4 \pm 0.5\ s^{-1}$) compared with H_2O ($k_{lim} = 57.4\ s^{-1}$), and a SIE ($=k_{lim}\ H_2O/k_{lim}\ ^2H_2O$) of 5.0 is observed at pH 4.0.[2] Enzyme-monitored turnover experiments performed in ^2H_2O yielded similar K_m values for spd and oxygen as in H_2O (data not shown), but a SIE of 2.3 was calculated from turnover values of 31.0 and 13.4 s^{-1} in H_2O and ^2H_2O, respectively. The turnover number in ^2H_2O (13.4 s^{-1}) determined from the enzyme-monitored turnover experiments is similar to that measured in single-turnover stopped-flow measurements at 450 nm (11.4 s^{-1}) under the same conditions, consistent with flavin reduction being the major contributor to the rate-limiting step in the overall catalysis. Our single-turnover and enzyme-monitored turnover studies suggest a key role for the active-site water molecule in the mechanism of flavin reduction.

Kinetic Constants of the Lys300Met MPAO Enzyme. We investigated further the involvement of Lys300 and HOH309 in the catalytic mechanism of MPAO by substituting Lys300 for a methionine residue in Lys300Met MPAO. This mutation disrupts the Lys300−H_2O−flavin N^5 hydrogen-bonding network seen in the structure of the wild-type enzyme. The Lys300Met MPAO mutant was purified from culture medium of *P. pastoris* and had a spectrum characteristic of oxidized FAD, indicating that flavin binding was not affected by the mutation. The circular dichroism spectrum of the Lys300Met MPAO mutant was comparable to that of the wild-type enzyme (not shown), indicating that this mutation did not interfere with the overall folding of the protein. Steady-state kinetic studies indicated that the substitution of Lys300 with Met300 led to a substantial loss of enzyme activity with both spd and spm (approximately 11 000-fold) (Table 1). Unexpectedly, the Michaelis constant of the Lys300Met enzyme was substantially diminished ($K_m < 0.1\ \mu M$) compared with the value measured for the recombinant wild-type enzyme, prompting a further study of flavin reduction (described below) using stopped-flow methods.

Kinetics of the Reductive Half-Reaction of the Lys300Met Enzyme. Stopped-flow studies of flavin reduction in Lys300Met MPAO were performed at pH 4.0 using spd as the substrate (Figure 4D). Absorption changes at 450 nm were monophasic at pH 4.0, and the limiting rate constant for flavin reduction ($k_{lim} = 0.040 \pm 0.001\ s^{-1}$) was ~1400-fold less than that measured for the wild-type enzyme (57 s^{-1}; Figure 4B). The equilibrium dissociation constant for the Lys300Met−spd complex was $18.2 \pm 3.0\ \mu M$. This value is 160-fold smaller than that measured for wild-type MPAO (2900 μM) and is consistent with the reduction in the Michaelis constant for the mutant enzyme in steady-state turnover. When our steady-state and stopped-flow studies of the Lys300Met enzyme are combined, they point to a major role for this residue in the mechanism of flavin reduction and in substrate binding.

Modeling of Wild-Type and Mutant MPAO−Substrate Complexes. To understand the structural and functional properties of MPAO that might give rise to the different catalytic properties of the Lys300Met mutant, we modeled the wild-type and Lys300Met mutant MPAO complexes with spm or spd using as a template the structure of the MPAO−MDL72527 and MPAO−1,8-diaminooctane complexes, respectively. MDL72527 and 1,8-diaminooctane (Figure 1B) are substrate homologues and are good inhibitors of MPAO (*9*, *10*). The models were relaxed through molecular dynamics simulations in explicit solvent. The wild-type MPAO enzyme−substrate complex structures obtained after molecular dynamics display conformations of spm and spd compatible with catalysis (Figure 6). In particular, the C^6

[2] Solvent isotope studies were performed on the plateau of the pH/pD curve ($pK_a = 5.8$), thereby ruling out contributions from isotope effects on the p*K* of the ionisable group. It is likely, therefore, that the measured SIE is related to the reaction itself, although an unequivocal demonstration of this would require a more detailed analysis.

Table 3: pK_a Values Calculated for the Active-Site Ionisable Groups of Wild-Type and Lys300Met MPAO in the Free-Enzyme and Enzyme−Substrate Complexes

	wild-type			Lys300Met		
	MPAO	MPAO−spm	MPAO−spd	MPAO	MPAO−spm	MPAO−spd
Glu62	>14.0	>14.0	>14.0	12.1	>14.0	>14.0
Glu170	11.5	10.8	8.5	7.5	<0.0	5.8
Tyr298	>14.0	>14.0	>14.0	>14.0	>14.0	>14.0
Lys300	8.8	4.2	5.8			
Tyr439	>14.0	>14.0	>14.0	>14.0	>14.0	>14.0
N^{1} [a]		0.0	<0.0		6.6	8.9
N^{5}		<0.0	<0.0		<0.0	<0.0
N^{10}		<0.0	>14.0		0.5	>14.0
N^{14}		8.5			>14.0	

[a] spm and spd atoms are numbered progressively starting from the inner (solvent-inaccessible) side of the MPAO catalytic site.

atom of spm and spd is ~4.0 Å from the N^5 atom of the enzyme-bound FAD. The Lys300−H_2O−FAD structural motif was stable throughout the MD simulations, with HOH309 bound to the N^5 atom of FAD by a strong hydrogen bond, with the distance between the FAD N^5 atom and the HOH309 H^1 atom being less than 2.7 Å. In the enzyme−substrate complexes formed by Lys300Met MPAO with spm and spd, we observed an increase in the distance of the C^6 atom to the FAD N^5 atom (5.1 and 5.2 Å, respectively). In addition, the hydrogen bond between HOH309 and the FAD N^5 atom is not retained in these complexes (Figure 6) because the water molecule moves away from the FAD by ~1 and ~2 Å in the complexes formed with spm and spd, respectively.

pK_a Calculations. We have calculated the protonation states of ionisable residues in substrate-free wild-type and Lys300Met MPAO and on the modeled enzyme−substrate complexes (Table 3). Calculations carried out on the substrate-free wild-type enzyme confirm the prediction, on the basis of 3D structure analysis (*9*), that the close proximity between Glu62 and Glu170 and the high negative charge density around the catalytic tunnel entrance stabilizes the protonated forms of both of these residues. Partial deprotonation of Glu62 and Glu170 is observed only at very basic pH values (pK_a > 14.0 and pK_a = 11.5, respectively). The prediction that both residues are protonated around physiological pH values is consistent with our kinetic studies of the Glu62Gln and Glu170Gln enzymes, which also suggest that both glutamate residues are protonated. Our calculations indicate that Lys300, the other ionisable residue found within the MPAO catalytic tunnel, has a "normal" pK_a of ~9.0 in the free enzyme. Binding of both spm and spd within the MPAO active site leads to a substantial decrease in the pK_a value for Lys300 to 4.2 and 5.8 for the MPAO−spm and MPAO−spd complexes, respectively. This major reduction in pK_a would be compatible with Lys300 acting as a catalytic base in these enzyme−substrate complexes. The pK_a of Glu62 is not affected by substrate binding, and only a small decrease in the pK_a of Glu170 is observed (values of 10.8 and 8.5 for the MPAO−spm and MPAO−spd complexes, respectively). As far as the protonation state of the substrates is concerned, the secondary amino groups are almost completely deprotonated over the whole pH range analyzed for both spm and spd (Table 3). This confirms that the charge distribution properties of the enzyme are consistent with the oxidation of the substrate when the secondary amino groups are in their deprotonated forms. Different degrees of protonation are observed between spm and spd for the terminal, solvent-accessible amino group. This deprotonates with a pK_a of 8.5 in the MPAO−spm complex but is fully protonated over most of the pH range analyzed in the MPAO−spd complex. In the substrate-free Lys300Met MPAO, both Glu62 and Glu170 have a lower pK_a value (pK_a of 12.1 and 7.5 for Glu62 and Glu170, respectively; Table 3) compared with the wild-type enzyme. This is attributed to an altered conformation of the two residues, which leads to a larger distance and lower electrostatic interaction energy between the two acidic groups (data not shown). In the mutant enzyme−substrate complexes, Glu62 is protonated over the entire pH range analyzed. However, Glu170 is deprotonated over the analyzed pH range in the MPAO−spm complex, whereas in the MPAO−spd complex, it deprotonates with a pK_a of 5.8 (Table 3). In regards to the substrate protonation state, major differences compared with the wild-type enzyme are observed only for the primary amino group buried within the tunnel. This is protonated at acidic pH values and deprotonates with a pK_a of 6.6 and 8.9 in the spm and spd complexes, respectively (Table 3).

DISCUSSION

The MPAO crystal structure (*9*, *10*) indicates that residues Glu62, Glu170, and Tyr298 are positioned inside the catalytic tunnel and protrude in front of the enzyme-bound flavin. We conjectured that these residues might be involved in catalysis by acting as a base for substrate oxidation and flavin reduction. Our studies presented in this paper, however, demonstrate that these residues do not play an essential role in the catalytic mechanism of MPAO. Specifically, replacement of Glu62 and Glu170 residues by the neutral analogue Gln and Tyr298 residue by Phe does not lead to major alterations in the catalytic activity and substrate affinity of the enzyme (Table 1). Our pK_a calculations carried out on the wild-type enzyme−substrate complexes have demonstrated that (i) the close proximity between Glu62 and Glu170 and (ii) the high negative charge density around the catalytic tunnel entrance stabilize the protonated form of both residues and that partial deprotonation occurs only at pH values greater than 8.0 (Table 3). The fact that both glutamate residues are protonated at physiological pH in the wild-type enzyme is also supported by the retention of wild-type levels of activity in the Glu62Gln and Glu170Gln enzymes. We conclude that neither Glu62, Glu170, nor Tyr298 play a major role in the catalytic mechanism of MPAO, thus ruling out roles as active-site bases in the oxidation of the substrate by the enzyme.

Lys300 is conserved in all PAOs sequenced thus far: the two barley PAO isoforms (*39*), the putative *Arabidopsis thaliana* PAO (Genbank accession number AB006704), animal PAOs (*2*, *4*, *5*), animal SMOs (*3*, *6*, *7*), and the yeast PAO Fms1 (*40*). In the X-ray crystal structure of oxidized MPAO, the Nϵ of Lys300 forms a hydrogen bond with HOH309, which in turn hydrogen bonds to the unprotonated N^5 atom of flavin. After reduction of the flavin cofactor by the substrate, the side chain of Lys300 is displaced by about 2 Å away from the flavin, which allows for reorientation of HOH309, enabling it to function as a hydrogen-bond acceptor with the protonated N^5 atom of reduced FAD (*10*). Interaction

of a lysine residue with the N^5 atom of FAD through a water "bridge" has also been observed in the structures of Fms1, the only other polyamine oxidase with known three-dimensional structure (*40*), and other flavoenzymes such as L-amino acid oxidase, monomeric sarcosine oxidase, and monoamine oxidase B (*41*). We have demonstrated that replacement of Lys300 with Met in MPAO lowers the rate of flavin reduction by at least 1400-fold compared to the wild-type enzyme. A major decrease is also observed in the overall steady-state catalytic activity of Lys300Met MPAO (Table 1). These findings are consistent with a major role for Lys300 in the catalytic mechanism of MPAO, specifically in the mechanism of substrate oxidation and FAD reduction. Substrate binding to the Lys300Met MPAO mutant is 160-fold tighter than to the wild-type enzyme at the same pH value, and a molecular basis for this observation is suggested from structural studies with MPAO inhibitors (*10*). The MPAO inhibitors guazatine and MDL72527 contain secondary amino groups but, unlike the substrate, are not oxidized by MPAO. A key factor in discriminating between the substrate and inhibitor molecules is the alignment of the C−N bond (the site of substrate oxidation) with the N^5 atom of the flavin isoalloxazine ring. Examination of various enzyme−inhibitor complexes indicates that the secondary amino groups and their adjacent carbon atoms are too far removed from the flavin N^5 atom to permit flavin-catalyzed oxidation. These inhibitors adopt an "out-of-register" mode of binding, which allows for tight binding but not catalysis. Similar observations might explain the kinetic results that we have obtained with the Lys300Met mutant. Replacement of Lys300 with Met in MPAO might result in a different conformation of the bound substrate in the Lys300Met mutant such that the substrate now adopts a more "inhibitor-like" mode of binding. In turn, this might account for the tighter binding of spd to the mutant enzyme. A consequence of the proposed different binding mode in the Lys300Met mutant is incorrect alignment of the C−N bond of the substrate with the flavin isoalloxazine ring, thus disfavoring substrate oxidation. A different conformation for the bound substrate in Lys300Met MPAO is supported by molecular dynamics simulations, which indicate an increased distance between the N^5 atom of FAD and the substrate carbon atom that is oxidized during catalysis. Our analysis of SIEs in stopped-flow and steady-state turnover studies of wild-type MPAO lends some support for a role for water HOH309 in catalysis, albeit ill-defined at this stage. Stopped-flow analysis revealed that a sizable SIE (=5) accompanies flavin reduction, and a SIE value of 2.3 is also observed in steady-state turnover of the wild-type enzyme. These data suggest that flavin reduction is rate-limiting in steady-state catalysis, a finding that is consistent with our observations of the flavin reduction state during enzyme-monitored turnover with the wild-type enzyme. It was also concluded that flavin reduction was the main contributor to rate limitation during steady-state turnover in mouse PAO, when kinetic studies revealed that the rate constant for flavin reduction (18.9 s^{-1}), measured with the substrate N^1,N^{12}-bisethylspermine, was comparable to the k_{cat} value (12.3 s^{-1}) calculated under the same conditions (*38*).

Theoretical calculations on modeled MPAO enzyme−substrate complexes indicate that the solvent inaccessibility of the MPAO active site gives rise to strong electrostatic effects that alter the acid−base properties of Lys300. After substrate binding, the pK_a of this residue is decreased ~4 pH units with respect to that in the free enzyme, yielding a pK_a value in the acidic pH range (Table 3). Thus, according to our calculations, at neutral pH, Lys300 has the properties of a strong base. Moreover, Lys300 appears to be the only ionisable residue within the MPAO active site to deprotonate around pH 5−6. Through calculation, we have shown that residues Tyr439 (Table 3) and Tyr169 (data not shown) have pK_a values higher than 14.0, and we have demonstrated by mutagenesis that neither Glu62, Glu170, nor Tyr298 represent the ionisable group governing the pH dependence observed in steady-state analysis of MPAO catalytic activity. The possibility remains that either Lys300 or HOH309, which is electrostatically linked to Lys300, might be the ionisable group with a pK_a of 5.7−5.8 (Table 2 and Figure 2). However, detailed analysis of the pH dependence will require careful evaluation of k_{cat}, K_m, and k_{cat}/K_m as a function of pH for wild-type and mutant enzymes and in H_2O and ^2H_2O, rather than relative activities as a function of pH as reported herein. These detailed studies are beyond the scope of the current paper.

An alternative explanation for the pH dependence of the MPAO activity, which is also consistent with the kinetic data, is that the ionization may belong to the substrate, i.e., deprotonation of the secondary amino group. The physiological substrates spm and spd are polycationic in nature because they contain both primary and secondary amino groups (Figure 1B). The pK_a value for deprotonation of the secondary amino group of free spd has been calculated as ~8.2 (*42*, *43*). The free substrate will therefore exist largely in the protonated form at neutral pH. In line with this, it has generally been assumed that the protonated form of the substrate (with both primary and secondary amino groups carrying a positive charge) binds to the enzyme (*9*, *10*, *44*). Modeling studies of MPAO enzyme−substrate complexes have indicated that the substrate secondary amino group is bound in an "aromatic cage" comprising the side chains of Tyr, Phe, and Trp residues, as well as the isoalloxazine ring of FAD (ref *16* and present study). The recognition of a substrate amine group by an "aromatic cage" has also been observed with trimethylamine dehydrogenase (*45*) and monoamine oxidase (*15*). For these enzymes and also for monomeric sarcosine oxidase (*46*), there is evidence to indicate that the enzyme preferentially binds the nonprotonated form of the substrate. In trimethylamine dehydrogenase, a substantial shift in the substrate pK_a on binding to the enzyme (pK_a of 6.5 for the enzyme−substrate complex compared with a pK_a of 9.8 for the free substrate; *25*, *26*) is observed. Likewise, the unprotonated form of the substrate is known to bind to monoamine oxidase (*24*, *47*, *48*). Mechanistic proposals for these enzymes are consistent with the unprotonated form of the substrate being the reactive species. In MPAO, the binding of the substrate secondary amine group within a hydrophobic environment could influence its ionization state and perturb the pK_a compared to the value observed in the bulk solvent, such that the pK_a decreases from ~8.2, in the free spd, to ~5.8 (the pK_a value similar of the group responsible for the pH dependence of flavin reduction) in the wild-type enzyme−substrate complex. The electronic environment of the substrate in the enzyme−substrate complex would be therefore crucial in

stabilizing the unprotonated form of the substrate. Theoretical pK_a calculations suggest that MPAO substrates are likely bound in the free-base form within the active site (Table 3). However, these calculations also suggest that the substrate secondary amino group is deprotonated over the whole pH range analyzed (i.e., pK_a < 0; Table 3), which would be inconsistent with this group being attributable to the kinetically influential ionization. This argues against the secondary amino group of the substrate being the ionisable group governing the observed pH dependence in kinetic studies of the enzyme. The mechanistic origin of the kinetically influential ionizations observed in steady-state studies of the enzyme remain to be elucidated, and this is the focus of future studies.

In summary, our work has established that Lys300 plays a major role in flavin reduction, which is manifested in steady-state turnover of the enzyme. The precise mechanistic role of this residue remains to be elucidated, and roles as an active-site base, modulator of flavin reduction potential, or modulator of the properties of HOH309 cannot be ruled out nor can involvement in the positioning of the substrate C−N close to the flavin N^5 atom. Our data supports a role as an active-site base, but further analysis is required to establish this unequivocally. Our work has also suggested a role for water in the mechanism of flavin reduction as inferred from SIE measurements. We have been able to eliminate major roles for Glu62, Glu170, and Tyr298 in the mechanism of flavin reduction and substrate binding and establish that Glu62 and Glu170 are likely to be protonated in the enzyme−substrate complex through a comparison of kinetic properties of the Glu62Gln and Glu170Gln enzymes. Our work has focused attention on the role of Lys300 in flavin reduction and now paves the way for more detailed evaluation of the role of this residue in enzyme catalysis.

ACKNOWLEDGMENT

We thank Prof. Andrea Mattevi, Prof. Andrea Bellelli, and Prof. Paolo Ascenzi for critical reading of the manuscript.

REFERENCES

1. Federico, R., and Angelini, R. (1991) Polyamine catabolism in plants, in *Biochemistry and Physiology of Polyamines in Plants* (Slocum, R. D., and Flores, H. E., Eds.) pp 41−56, CRC Press, Boca Raton, FL.
2. Seiler, N. (1995) Polyamine oxidase, properties and functions, *Prog. Brain Res. 106*, 333−344.
3. Vujcic, S., Diegelman P., Bacchi, C. J., Kramer, D. L., and Porter, C. W. (2002) Identification and characterization of a novel flavin-containing spermine oxidase of mammalian cell origin, *Biochem. J. 367*, 665−675.
4. Wu, T., Yankovskaya, V., and McIntire, W. S. (2003) Cloning, sequencing, and heterologous expression of the murine peroxisomal flavoprotein, N^1-acetylated polyamine oxidase, *J. Biol. Chem. 278*, 20514−20525.
5. Vujcic, S., Liang, P., Diegelman, P., Kramer, D. L., and Porter, C. W. (2003) Genomic identification and biochemical characterization of the mammalian polyamine oxidase involved in polyamine back-conversion, *Biochem. J. 370*, 19−28.
6. Wang, Y., Devereux, W., Woster, P. M., Stewart, T. M., Hacker, A., and Casero, R. A., Jr. (2001) Cloning and characterization of a human polyamine oxidase that is inducible by polyamine analogue exposure, *Cancer Res. 61*, 5370−5373.
7. Cervelli, M., Polticelli, F., Federico, R., and Mariottini, P. (2003) Heterologous expression and characterization of mouse spermine oxidase, *J. Biol. Chem. 278*, 5271−5276.
8. Tavladoraki, P., Shinina, M. E., Cecconi, F., Di Agostino, S., Manera, F., Rea, G., Mariottini, P., Federico, R., and Angelini, R. (1998) Maize polyamine oxidase: Primary structure from protein and cDNA sequencing, *FEBS Lett. 426*, 62−66.
9. Binda, C., Coda, A., Angelini, R., Federico, R., Ascenzi, P., and Mattevi, A. (1999) A 30-Å long U-shaped catalytic tunnel in the crystal structure of polyamine oxidase, *Structure 7*, 265−276.
10. Binda, C., Angelini, R., Federico, R., Ascenzi, P., and Mattevi, A. (2001) Structural bases for inhibitor binding and catalysis in polyamine oxidase, *Biochemistry 40*, 2766−2776.
11. Dailey, T. A., and Dailey H. A. (1998) Identification of an FAD superfamily containing protoporphyrinogen oxidases, monoamine oxidases, and phytoene desaturase, *J. Biol. Chem. 273*, 13658−13662.
12. Shih, J. C., Chen, K., and Ridd, M. J. (1999) Monoamine oxidase: From genes to behavior, *Annu. Rev. Neurosci. 22*, 197−217.
13. Cesura, A. M., and Pletscher, A. (1992) The new generation of monoamine oxidase inhibitors, *Prog. Drug Res. 38*, 171−297.
14. De Zutter, G. S., and Davis, R. J. (2001) Pro-apoptotic gene expression mediated by the p38 mitogen-activated protein kinase signal transduction pathway, *Proc. Natl. Acad. Sci. U.S.A. 98*, 6168−6173.
15. Binda, C., Newton-Vinson, P., Hubalek, F., Edmondson, D. E., and Mattevi, A. (2002) Structure of human monoamine oxidase B, a drug target for the treatment of neurological disorders, *Nat. Struct. Biol. 9*, 22−26.
16. Fraaije, M. W., and Mattevi, A. (2000) Flavoenzymes: Diverse catalysts with recurrent features, *Trends Biochem. Sci. 25*, 126−132.
17. Jang, M.-H., Basran, J., Scrutton, N. S., and Hille, R. (1999) The reaction of trimethylamine dehydrogenase with trimethylamine, *J. Biol. Chem. 274*, 13147−13154.
18. Mattevi, A., Vanoni, M. A., Todone, F., Rizzi, M., Teplyakov, A., Coda, A., Bolognesi, M., and Curti, B. (1996) Crystal structure of D-amino acid oxidase: A case of active site mirror-image convergent evolution with flavocytochrome b_2, *Proc. Natl. Acad. Sci. U.S.A. 93*, 7496−7501.
19. Umhau, S., Pollegioni, L., Molla, G., Diederichs, K., Welte, W., Pilone, M. S., and Ghisa, S. (2000) The X-ray structure of D-amino acid oxidase at very high-resolution identifies the chemical mechanism of flavin-dependent substrate dehydrogenation, *Proc. Natl. Acad. Sci. U.S.A. 97*, 12463−12468.
20. Silverman, R. B. (1991) The use of mechanism-based inactivators to probe the mechanism of monoamine oxidase, *Biochem. Soc. Trans. 19*, 201−206.
21. Edmondson, D. E. (1995) Aminium cation radical mechanism proposed for monoamine oxidase B catalysis: Are there alternatives? *Xenobiotica 25*, 735−753.
22. Walker, M. C., and Edmondson, D. E. (1994) Structure−activity relationships in the oxidation of benzylamine analogues by bovine liver mitochondrial monoamine oxidase B, *Biochemistry 33*, 7088−7098.
23. Kim, J.-M., Bogdon, M. A., and Mariano, P. S. (1993) Mechanistic analysis of the 3-methyllumiflavin-promoted oxidative deamination of benzylamine. A potential model for monoamine oxidase catalysis, *J. Am. Chem. Soc. 115*, 10591−10595.
24. Miller, J. R., and Edmondson, D. E. (1999) Structure−activity relationships in the oxidation of para-substituted benzylamine analogues by recombinant human liver monoamine oxidase A, *Biochemistry 38*, 13670−16683.
25. Basran, J., Sutcliffe, M. J., and Scrutton, N. S. (2001) Deuterium isotope effects during C−H bond cleavage by trimethylamine dehydrogenase: Implications for mechanism and vibrationally assisted H-tunneling in wild-type and mutant enzymes, *J. Biol. Chem. 276*, 24581−24587.
26. Basran, J., Sutcliffe, M. J., and Scrutton, N. S. (2001) Optimizing the Michaelis complex of trimethylamine dehydrogenase. Identification of interactions that perturb the ionization of substrate and facilitate catalysis with trimethylamine base, *J. Biol. Chem. 276*, 42887−42892.
27. Scrutton, N. S. (2004) Chemical aspects of amine oxidation by flavoprotein enzymes, *Nat. Prod. Rep. 21*, 722−730.
28. Federico, R., Alisi, C., and Forlani, F. (1989) Properties of the polyamine oxidase from the cell wall of maize seedlings, *Phytochemistry 28*, 45−46.
29. Holt, A., and Baker, G. B. (1995) Metabolism of agmatine (clonidine-displacing substance) by diamine oxidase and the possible implications for studies of imidazoline receptors, *Prog. Brain Res. 106*, 187−197.

30. Leatherbarrow, R. J. (1992) *Grafit*, version 3, Erithacus Software Ltd., Staines, U.K.
31. Gibson, Q. H., Swoboda, B. E. P., and Massey, V. (1964) Kinetics and mechanism of action of glucose oxidase, *J. Biol. Chem. 239*, 3927−3934.
32. Brooks, B. R., Bruccoleri, R. E., Olafson, B. D., States, D. J., Swaminathan, S., and Karplus, M. (1983) CHARMM: A program for macromolecular energy, minimization, and dynamics calculations, *J. Comput. Chem. 4*, 187−217.
33. MacKerell, A. D., Jr., Bashford, D., Bellott, M., Dunbrack, R. L., Jr., Evanseck, J. D., Field, M. J., Fischer, S., Gao, J., Guo, H., Ha, S., Joseph-McCarthy, D., Kuchnir, L., Kuczera, K., Lau, F. T. K., Mattos, C., Michnick, S., Ngo, T., Nguyen, D. T., Prodhom, B., Reiher, W. E., III, Roux, B., Schlenkrich, M., Smith, J. C., Stote, R., Straub, J., Watanabe, M., Wiorkiewicz-Kuczera, J., Yin, D., and Karplus, M. (1998) All-atom empirical potential for molecular modeling and dynamics studies of proteins, *J. Phys. Chem. B 102*, 3586−3616.
34. Jorgensen W. L., Chandrasekhar, J., Madura, J., Impley, R. W., and Klein, M. L. (1983) Comparison of simple potential functions for simulating liquid water, *J. Chem. Phys. 79*, 926−935.
35. Alexov, E. G., and Gunner, M. R. (1997) Incorporating protein conformational flexibility into the calculation of pH-dependent protein properties, *Biophys. J. 72*, 2075−2093.
36. Alexov, E. G., and Gunner, M. R. (1999) Calculating protein and proton motions coupled to electron transfer: The electron transfer from QA to QB in photosynthetic reaction centers from *Rb. sphaeroides*, *Biochemistry 38*, 8253−8270.
37. Georgescu, R. E., Alexov, E. G., and Gunner, M. R. (2002) Combining conformational flexibility and continuum electrostatics for calculating pK_a's in proteins, *Biophys. J. 83*, 1731−1748.
38. Royo, M and Fitzpatrick P. F. (2005) Mechanistic studies of mouse polyamine oxidase with N^1,N^{12}-bisethylspermine as a substrate, *Biochemistry 44*, 7079−7084.
39. Cervelli, M., Cona, A., Angelini, R., Polticelli, F., Federico, R., and Mariottini, P. (2001) A barley polyamine oxidase isoform with distinct structural features and subcellular localization, *Eur. J. Biochem. 268*, 3816−3830.
40. Huang, Q., Liu, Q., and Hao, Q. (2005) Crystal structures of Fms1 and its complex with spermine reveal substrate specificity, *J. Mol. Biol. 348*, 951−959.
41. Binda, C., Mattevi, A., and Edmondson, D. E. (2002) Structure−function relationships in flavoenzyme-dependent amine oxidations, *J. Biol. Chem. 277*, 23973−23976.
42. Delfini, M., Segre, A. L., Conti, F., Barbucci, R., Barone, V., and Ferruti, P. (1980) On the mechanism of protonation of triamines, *J. Chem. Soc., Perkin Trans. 2*, 900−903.
43. Gold, M., and Powell, H. K. J. (1976) Thermochemical study of the stepwise protonation of 3-azaheptane-1,7-diamine and 4-azaoctane-1,8-diamine, and of complex formation between copper(II) and 3-azaheptane-1,7-diamine and 4,9-diazadodecane-1,12-diamine, *J. Chem. Soc., Dalton Trans. 3*, 230−233.
44. Cona, A., Manetti, F., Leone, R., Corelli, F., Tavladoraki, P., Polticelli, F., and Botta, M. (2004) Molecular basis for the binding of competitive inhibitors of maize polyamine oxidase, *Biochemistry 43*, 3426−3435.
45. Lim, L. W., Shamala, N., Mathews, F. S., Steenkamp, D, J., Hamlin, R., and Xuong, N. (1986) Three-dimensional structure of the iron−sulfur flavoprotein trimethylamine dehydrogenase at 2.4 Å resolution, *J. Biol. Chem. 261*, 15140−15146.
46. Zhao, G., and Jorns, M. J. (2002) Monomeric sarcosine oxidase: Evidence for an ionizable group in the E·S complex, *Biochemistry 41*, 9747−9750.
47. McEwen, C. M., Sasaki, G., and Lenz, W. R. (1968) Human liver mitochondrial monoamine oxidase. I. Kinetic studies of model interactions, *J. Biol. Chem. 25*, 5217−5225.
48. McEwen, C. M., Sasaki, G., and Jones, D. C. (1969) Human liver mitochondrial monoamine oxidase. II. Determinants of substrate and inhibitor specificities, *Biochemistry 8*, 3952−3962.
49. Nicholls, A., Sharp, K. A., and Honig, B. (1991) Protein folding and association: Insights from the interfacial and thermodynamic properties of hydrocarbons, *Proteins 11*, 281−296.

BI050983I